Egypt. J. Chem. **Vol. 65,** No. SI:13B pp. 443 - 453 (2022)

Egyptian Journal of Chemistry

http://ejchem.journals.ekb.eg/

Influence of Aluminum Cations on the Structural, Optical and Electrical Properties of ZnO Nanopowder

N.M. Moussa*[a], F.M. Ebrahim[a], Hosam M. Gomaa[c], K. Adly[b], and M.Y Hassaan[a]

a. *Physics Department, Faculty of Science, Al-Azhar University, Cairo, Egypt*

b. *Physics Department, Faculty of Science. Suez Canal University, Ismailia, Egypt*

c. *Basic Science Department, Pharaohs-Higher Institute for Computer, Information Systems and Management, Giza, Cairo, Egypt*

Abstract

This research work aims to prepare and characterize the effect of Al-doped ZnO nanoparticles (NPs) from the point of view of different physical properties for different applications. The co-precipitation method was used for preparing the desired samples, where ZnO was replaced by $AlCl_3$. The obtained samples were characterized using both Fourier transform infrared (FTIR) and X-ray diffraction (XRD) to identify their structural phases. All samples exhibit a single-phase hexagonal wurtzite structure confirming the substitution of Al on Zn sites. The average crystallite size was found to increase for all Al-doped ZnO samples. UV-vis spectra showed an absorption peak around 3.34 eV which matches the optical bandgap of ZnO. Al-Impurities acted to increase the value of the optical transmittance, especially in the visible light region. The value of the calculated nonlinear refractive index is considered promising for different optoelectronic applications. In addition, the electrical conductivity of Al-doped ZnO samples increased at a high frequency compared with that of pure ZnO due to the increase of available charge carriers after the replacement of Zn ions by Al ions. Also, dielectric constant and loss (tan δ) was found to be frequency-dependent.

Keywords: ZnO, nanoparticles, optical properties, electrical conductivity

1. Introduction

Nanomaterials and Nanocomposites are of high importance in different fields because of their potential applications, such as storage energy devices, optoelectronic instruments, and solar cells. for example, Nanoparticles based on ZnO have been used as a drug-delivery active medium in UV-region semiconductor lasers [1-6], where zinc oxide is a semiconductor oxide that has a wide direct bandgap of about 3.37 eV, and a large exciton binding energy of about 60 m eV [2, 3], at room temperature. Large numbers of publications stated that Nanoparticles based on Zinc metal oxide with or without another metal oxide or more is considered as one of the most unique ways that provide what is called long-lasting superior protection [7-9]. Also, it was found that when ZnO nanopowder mixes with other different ions acts to improve the optical, electrical, and catalytic properties of these ions [9], especially, when ZnO nanopowder is doped with Al, where the resulted compound is conductive and transparent in the visible region, which suggests it be used in the transparent conductive pastes [10–11]. Therefore, in recent years the most researchers in the area of material science focused to develop new technics and experimental methods to obtain and fabricate ZnO nanostructures, like the co-precipitation, sol-gel, hydrothermal, and spray pyrolysis [12-13], Among all developed techniques the co-precipitation technique has attracted more attention because of its simplicity as well as its low cost, and effectiveness. Through inspecting the related previous articles, it was found that ZnO nanopowder doped with Al, has been reported only by a small number of researchers especially their optical properties in the UV-vis-near IR region. Most research works aimed to prepare the Al-doped ZnO powders based on the sol-gel method, where it was found that the incorporation of Al^{3+} ions into Zn^{2+} lattice resulted in the reduction of the crystalline nature of ZnO, such reduction act to increase the value of the optical bandgap [14-18]. Accordingly, this study has been performed to try to prepare Al-free and Al-doped ZnO nanopowder using the co-precipitation method, then estimate the effect of Al-doping on structural and optical properties of ZnO nanopowder based on the new preparation procedure.

Experimental Work:

Pure and Al-doped [Al_x $Zn_{(1-x)}$] samples were prepared by the chemical co-precipitation method. The used materials are commercial grade (LOBA Chemical) without any purification including Zinc acetate

*Corresponding author e-mail: xpnasser@yahoo.com.; (N. M. Moussa).

Receive Date: 31 March 2022, Revise Date: 06 May 2022, Accept Date: 21 May 2022

DOI: 10.21608/EJCHEM.2022.130786.5756

dehydrate [Zn $(CH_3COO)_2$ $.2H_2O$, purity 98%], sodium hydroxide [NaOH, purity 93%], Aluminum chloride Anhydrous ($AlCl_3$). As shown in figure (1a), the experimental procedure for the preparation of both pure ZnO sample and Al-doped ZnO samples are as follows: for the preparation of pure ZnO nanoparticles, 21.950 g of Zinc Acetate was dissolved in 100 ml distilled water, and a magnetically stirred at room temperature (RT) to obtain a homogenous solution, then 16 g of sodium hydroxide was dissolved in 100 ml distilled water. Next NaOH solution was added dropwise to obtain a homogenous mixed solution, yielding a white precipitate. The white precipitate was stirred at room temperature for 2 hours. After that, the product precipitates were then filtered out and washed several times with ethanol and distilled water.

The white powder was dried at 70 ºC for 3 hours followed by further heating at 400 ºC for 4 hrs to ensure good crystallinity of formed nanoparticles. Finely the white powder was ground using agate mortar. For the synthesis, Al-doped samples, the amount of $AlCl_3$ [0.53336 g (0.04), 0.80004 g (0.06), and 1.0667 g (0.08) were dissolved in (20ml) distilled water and added to (21.072 g) of zinc acetate dissolved in (80ml) distilled water with continues stirring both solutions for two an hour. Then (16g) of sodium hydroxide which dissolved in (100ml) distilled water was added dropwise to this homogenous mixture to form a white precipitate. The solution with the white precipitate was processed as above to obtain Al-doped ZnO samples, as seen in figure (1b). Eventually, all samples were coded as shown in table (1). The prepared samples were then characterized using different experimental methods, like the Powder X-ray diffractometer (XRD), at room temperature using a PW 1830 diffractometer with Cu Kα radiation (40 kV X 25 mA) and a graphite monochromatic, with 2θ values from 10 to 80 degrees. The optical measurements were obtained using Genway 6405-UV–visible Spectrophotometer which was used to get the optical UV–vis. Spectra, in the range 190 to 900 nm, at room temperature, using equal thickness samples (0.25 cm). While the FTIR spectra were recorded, at room temperature, using Fourier transform Infrared (FTIR) spectrometer in the range from 4000 to 400 cm^{-1}.

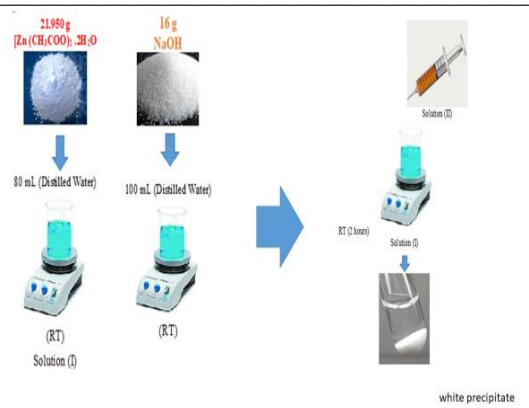

Fig. (1a): Schematic diagram for the experimental preparation of ZnO nanopowder sample

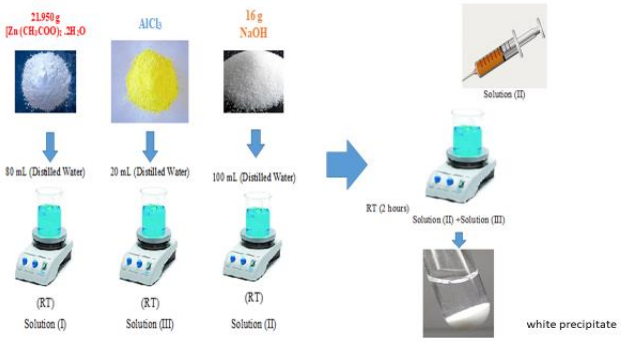

Fig. (1b): Schematic diagram for the experimental preparation of Al-doped samples

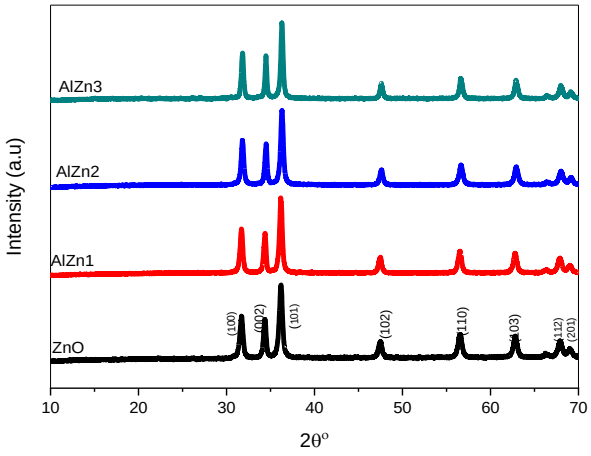

Fig (2): X-ray diffraction patterns for all the prepared samples ZnO, $AlZn_1$, $AlZn_2$, and $AlZn_3$.

Table (1): XRD peaks positions & their corresponding crystalline planes

2θº	32	34	36	48	57	63	68	69	Refs.
	Assignments								
ZnO $AlZn_1$ $AlZn_2$ $AlZn_3$	100	002	101	102	110	103	112	201	[19, 20, 21]

Results and Discussion

Structural Phase Identification by XRD:

Figure (2) shows the XRD patterns of Al-free and Aluminum-doped samples, it's clear that each pattern consists of eight sharp peaks of different amplitudes and different positions. Where each peak characterizes a certain crystalline plane (hkl), which in turn distinguishes one structural phase.

By inspecting the previous related publications, all the diffraction peaks have been attributed to their corresponding crystalline planes, as shown in table (1). Based on the standard data referred to as JCPDS card No. 36 –145, all data tabulated in table (1) can be attributed to the ZnO wurtzite hexagonal structure. Therefore, based on XRD results it can be stated that ZnO nano-powders have a polycrystalline hexagonal wurtzite structure with a well-developed crystallinity degree. Such behavior indicates that Al^{3+} ions occupied the sites of Zn^{2+} ions and/or incorporated into interstitial sites in the lattice without altering the hexagonal wurtzite structure of ZnO [22]. Also, figure (2) illustrates that when the content of Al^{3+} increased up to 8wt% the observed peaks exhibited a slight shift towards the higher diffraction angle 2θ°, as declared in figure (3). Like behavior may be due to the lattice shrinkage caused by the Al^{3+} (radius 0.53 ˚A) replacing the Zn^{2+} (radius 0.74 ˚A) [23-26]. Sharer equations (1, 2) have been used to obtain both the average crystal size (D) and the micro-strain (ε) values, for all samples. Where β is the full width at half maximum (FWHM) of the peak, θ is the Bragg's diffraction angle, K is the shape factor (K = 0.9), λ is the wavelength for CuKα radiation (λ = 1.54056 Å).

$$D = \frac{K\lambda}{\beta \cos\theta} \quad (1)$$

$$\varepsilon = \frac{\beta}{4 \tan\theta} \quad (2)$$

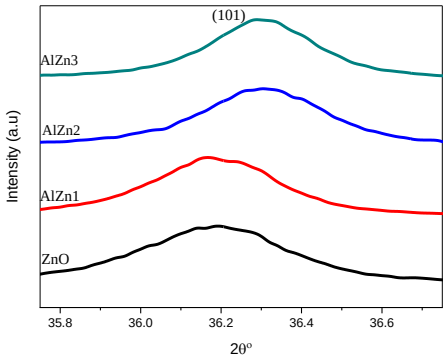

Fig. (3): Detail observation of the peak position (101) plane for all samples, ZnO, AlZn1, AlZn2, and AlZn3.

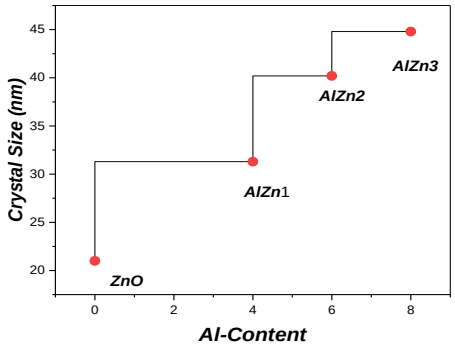

Fig. (4). Crystal size versus Al concentration

Table (2): Composition & structure information

Sample abbreviation		ZnO	$AlZn_1$	$AlZn_2$	$AlZn_3$
Samples chemical compositions		$Al_x Zn_{1-x}$ where x = 0, 4, 6, 8 (g)			
Crystallite size D (nm)		28.01	34.24	40.18	43.87
Dislocation density δ		0.001274	0.0008529	0.0006194	0.0005195
Micro-strain, ε ×10^{-3}		6.537	5.627	5.639	4.767
Lattice parameters	a (Å)	3.2571	3.2573	3.2455	3.2455
	c (Å)	5.2164	5.2153	5.1973	5.1981
	c/a	1.6015	1.6011	1.6013	1.6016
	u	0.3798	0.3800	0.3799	0.3799
	Cell-Volume (Å^3)	47.92	47.91	47.4	47.41
	Bond length (Å)	1.9815	1.9819	1.9747	1.9747

Table (2) exhibits the calculated average crystalline size as well as the corresponding lattice strain. As shown in figure (4), it can be seen that the average crystallite size increased when Al content increased, which may be due to the incorporation of Al in the ZnO Lattice acting to enhance its crystalline quality. This expectation has been confirmed by the observed decrease in the values of the micro-strain as shown in table (2).

$$\frac{1}{d^2} = \frac{4}{3}\left(\frac{h^2 + hk + k^2}{a^2}\right) + \frac{l^2}{c^2} \quad (3)$$

$$n\lambda = 2d\sin\theta \quad (4)$$

$$V = \frac{\sqrt{3}}{2} a c^2 \quad (5)$$

$$l = \sqrt{\left(\frac{a^2}{3} + \left(\frac{1}{2} - u\right)^2 c^2\right)} \quad (6)$$

$$u = \frac{1}{3}\left(\frac{a^2}{c^2}\right) + \frac{1}{4} \quad (7)$$

The equation of inter-planer spacing for a tetragonal unit cell is given by equation (3) [28] has been used to calculate the lattice parameters (a) and (c), as well as the unit cell volume for all samples. Where d is the inter-planar spacing and the h, k and l are the miller indices d-spacing is given by Bragg's law, Where λ =1.5406 Å, θ is the diffraction angle, n=1 (order of diffraction). The Zn–O bond length along the c-direction is given by [30], while the volume V of the

unit cell of the hexagonal wurtzite structure of the ZnO (NP_S), is obtained from Eq (5), [29]. The positional parameter 'u', which is an important variable in calculating the Zn–O bond length is given by Equation (7), [31].

The values of lattice parameters, unit cell volume, bond length (*l*), and (u) of ZnO and Al-doped ZnO nanoparticles are tabulated in table (2). All these quantities have been discussed separately as follows; (a) the lattice parameters (a, c, c/a) showed slight changes with the different Al-doping concentrations. Such slight changes of (a, c) parameters mean that the doping process affected the internal structure of ZnO (NP_S). (b) The unit cell volume, and bond length (*l*) of Al-free and Al-doped ZnO nanoparticles showed nominal different changes. These changes may be attributed to the difference between the atomic radii of Al and Zn atoms, where the atomic radius of Al atoms (0.118 nm) is smaller than that of Zn atoms (0.142 nm) and Al-O covalent bond length is shorter than Zn-O bond length, that leading to decrease in unit cell dimensions of Al-doped ZnO nanoparticles.

FT-IR Spectral Analysis:

Figures 5(a-d) exhibit the charts of Fourier-transform infrared spectroscopy, FTIR, for all as-prepared samples in the range of wavenumbers 400-4000 cm^{-1}. Such charts reveal the existence of multi absorption peaks, each peak and shoulder peak represents a certain vibrational mode. Based on the related previous publications, each peak has been assigned to a group function or a chemical bond as shown in table (3), where the observed peaks were classified into main bands. The absorption band 440-477 cm^{-1} has been assigned to the stretching vibrational modes of ZnO, the relative intensity of such band decreased as the content of Al-impurities increased the thing which may be assigned to the relative decrease in the content of Zn^{2+} cations. The center of such band shifted to the higher wavenumber as the Al-impurities increased, which means an increase in the bond energy of Zn-O and in turn decrease in its bond length and confirms what resulted from the XRD analysis which declared a decrease in the value of the lattice parameter (a) from 1.9815 to 1.9747 Å. The peak which is centered at 570 cm^{-1} distinguishes the metal cation (Zn^{2+} and Al^{3+}) vibrations. This band became broad as the Al-impurities content increased the thing which may refer to the participation of some Al^{3+} in ZnO-lattice. Such behavior may explain the increase in the value of the crystallite size D from 28.1 to 43.87 nm. The stretching mode of vibration bands due to C=O is observed between 1600-1400 cm^{-1}. While the broadband of absorption that was observed at 1097 cm^{-1}, 1384 cm^{-1}, and 840 cm^{-1} due to the effect of the presence of H_2O (O-H) and CO_2 (C-O) absorbed from the air, so can be ignored. Finally, it's obvious that the OH-groups gradually replaced with acetate groups, which disappear completely to form Zn $(OH)_2$, and hence/finally ZnO could be formed with the release of more acetate anion [33].

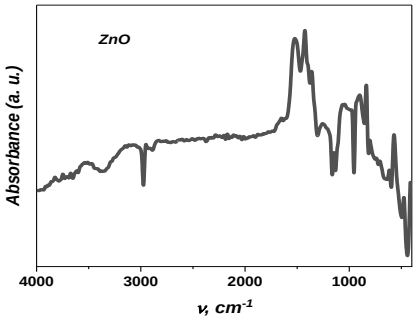

Fig. (5a): FTIR spectra for Al-free sample

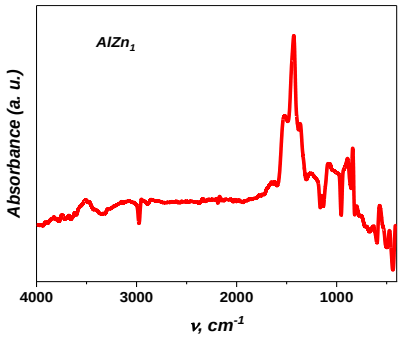

Fig. (5b): FTIR spectra for Al-doped sample (x = 0.04)

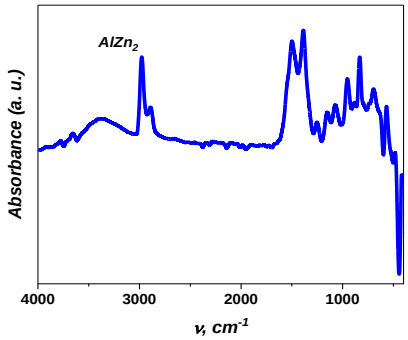

Fig. (5c): FTIR spectra for Al-doped sample (x = 0.06)

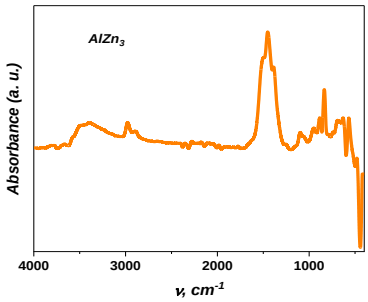

Fig. (5d): FTIR spectra for Al-doped sample (x = 0.08)

Table (3): FTIR Absorption peaks positions

Peak center	Assignments	Refs.
477 cm^{-1}	This peak corresponds to the stretching mode of ZnO vibration	[30-33]
570 cm^{-1}	Such peak can be attributed to the presence of Al cations throughout the ZnO lattice	
1600-1400 cm^{-1}	This band represents the stretching mode of vibration bands due to C=O vibrations	
Above1600 cm^{-1}	due to the presence of H_2O (O-H) and CO_2 (C-O) that are absorbed from the air, so can be ignored	

UV-Vis: Optoelectronic Analysis:

The study of non-Centro-Symmetric substances like ZnO nanopowder is of most importance in estimating the electronic structure according to the optical properties, which are of high importance in updating both the electronics and optoelectronic devices for the different applications. In the current study, some optical parameters like the transmittance (T %) and absorbance (A) were measured, while some others like absorption coefficient, linear refractive, and nonlinear refractive index were calculated [33-35]. For the studied samples, both the optical absorbance and optical transmittance were measured and then normalized, by dividing the highest value, to avoid the instrumental errors.

Figure (6) showed the variation of the normalized optical absorbance (A) with the change in the wavelength of the incident light, where all samples exhibit approximately the same cut-off wavelength around 293 nm, in addition to an absorption peak at 373 nm which represents the optical bandgap of ZnO in the UV region. The observed increase in the value of (A) as the Al-impurities increase may be attributed to the decrease in the value of the lattice parameter (a) as well as the decrease in the value of the bond length. Where these two factors refer to an increase in structure competence as Al-impurities which in turn may cause an increase in the density value which leads to an increase in the value of the optical absorbance. Also, the increase in the content of Al-impurities introduces more free charges and increases the probability of the electronic transitions which indeed increases the value of the optical absorbance.

Figure (6) also clarify the effect of Al content on the optical absorption, where the increase of Al-content act to increase the optical absorption, such an increase may be due to the observed increase in the average crystal size, as shown in figure (3). Figure (7) illustrates that all the studied samples have a wide transmission window extended over all the visible range, which may suggest them for multi applications in this region. According to relation (8), [36], both the optical absorption of each sample and its thickness (t) were used to calculate its absorption coefficient α, which is an important factor for determining the energy bandgaps for both direct and indirect allowed transitions, by using Tauc's relation (9), [37-38]; Where (α_o) is a constant called band tailing parameter, (E_g) is the optical energy gap, and (j) is the power factor of the transition mode. The values of (j) for both direct and indirect transitions are ½ and 2, respectively.

$$\alpha = 2.303 * \frac{A}{t} \quad (8)$$

$$\alpha E = \alpha_o (E - E_g)^j \quad (9)$$

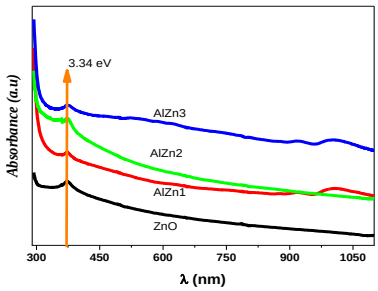

Fig. (6): Normalized Absorbance, for all the prepared samples, ZnO, $AlZn_1$, $AlZn_2$, and $AlZn_3$

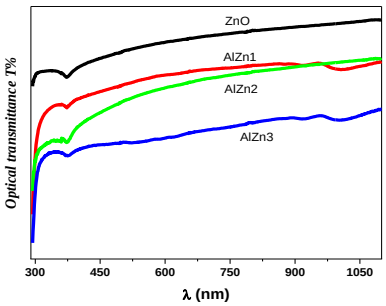

Figure (7): The optical transmittance T%, for all the prepared samples ZnO, $AlZn_1$, $AlZn_2$, and $AlZn_3$

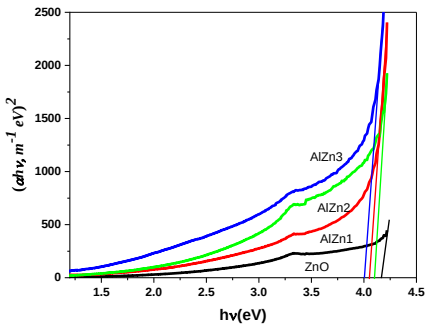

Fig. (8): $(\alpha h\upsilon)^2$ versus (E), for all the prepared samples, ZnO, $AlZn_1$, $AlZn_2$, and $AlZn_3$

To determine the value of the energy bandgap for the direct bandgap energy is equal to the intercept of the straight portion curve with the x-axis, it can determine the value of the bandgap energy for the direct allowed transition by plot $(\alpha h\upsilon)^2$ versus E= (hυ eV), as shown in figure (8). The calculations showed that the replacement of ZnO by $AlCl_3$ acts to increase the optical bandgaps from 4.01 to 4.17 eV for the direct allowed electronic transitions. Based on the measured optical parameters the optical dielectric relaxation can be organized given the real (ε_1) and imaginary (ε_2) components of the optical dielectric constant ε* [39-40]. Whereas for an un-free damper, the real component (ε_1) characterizes the damping of the light propagation through the material/medium. Also, this component, which is related to the energy stored within the medium, can be considered as an account for electromagnetic dispersions. On the other side, the imaginary component is considered a damping factor that describes the amount of energy loss and/or absorbed within the medium [39-40].

$$K(E) = \frac{\alpha\, hc}{4\pi E} \quad (10)$$

$$R = \frac{100-A-T\%}{100} \quad (11)$$

$$n = \frac{1+R}{1-R} + \sqrt{\frac{4R}{(1-R)^2} + K^2} \quad (12)$$

$$\varepsilon_2 = n^2 - K^2 \quad (13)$$

$$\varepsilon_2 = 2\,nK \quad (14)$$

$$\varepsilon^* = \varepsilon_1 + j\,\varepsilon_2 \quad (15)$$

Figure 9(a-d) represents the vibration of ε_1 and ε_2 with the energy of the incident photons for x = 0, 0.04, 0.06, and 0.08, respectively. Where the real component ε_1 increases while the imaginary component (ε_2') decreased, in such a way that both of them show a peak in the same position of photon energy (3.3 eV). Such a result can be used to obtain the average plasma frequency $f_o = 8\,x\,10^{14}\,Hz$ which is a higher value that gives the existence of a high concentration of free carriers [39].

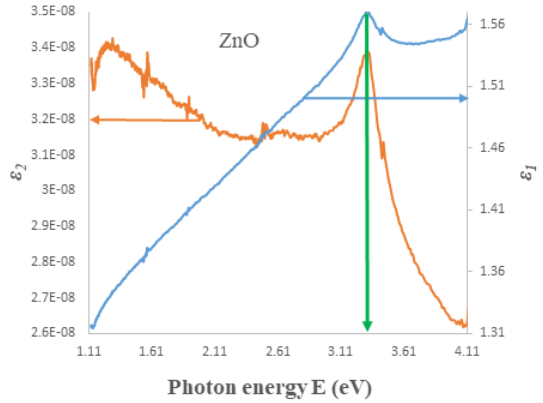

' Fig. (9a): (ε_1) and (ε_2) as a function of the photon energy for the sample x= 0.0wt%.

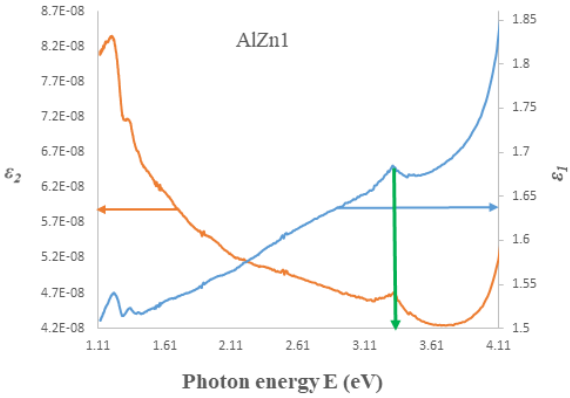

Fig. (9b): (ε_1) and (ε_2) as a function of the photon energy for the sample x= 0.04wt%.

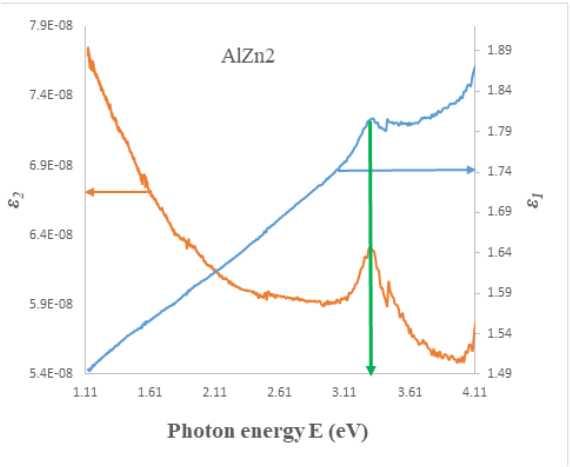

Fig. (9c): (ε_1) and (ε_2) as a function of the photon energy for the sample of x=0.06wt%.

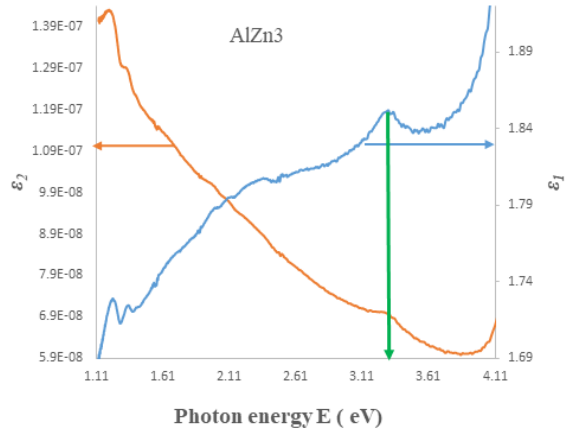

Fig. (9d): (ε_1) and (ε_2) as a function of the photon energy, for the sample x= 0.08wt%.

Nonlinear Refractive Index:

$$\chi^{(1)} = \frac{n^2-1}{4\pi} \quad (16)$$

$$\chi^{(3)} = 1.7\,x\,10^{-10}\,(\chi^{(1)})^4 \quad (17)$$

$$n_2 = \frac{12\pi\,\chi^{(3)}}{n} \quad (18)$$

Frequency conversion materials especially nanopowder semiconductors are important for

nonlinear optical applications, so it is useful to identify the nonlinear properties of the studied samples to recognize if they are suitable for nonlinear devices and applications or not. For this promotion, it's favorable to use the Z-scan technique but it's not available for now at least so the set of the previous relations should be used to obtain the nonlinear parameters of the studied samples based on UV-vis measurements. Figure (10) shows the calculated nonlinear refractive index n2, where the obtained values for the Al-free sample and Al-doped samples are better than those reported previously [40-41], which may suggest these samples for nonlinear applications.

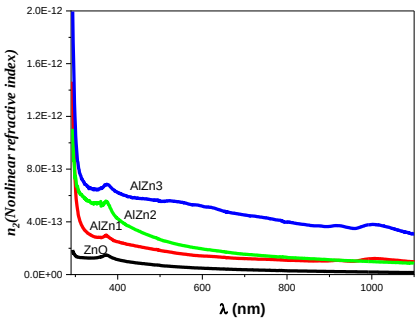

Fig. (10). Nonlinear refractive index n_2 for all samples, ZnO, $AlZn_1$, $AlZn_2$, and $AlZn_3$

Dielectric Relaxation:

The dielectric permittivity ε* is a complex quantity consisting of a real part which is named the dielectric constant ε' and an imaginary part which is named dielectric loss ε", relation (19) [42]. Figure (11) and figure (12) display the applied frequency impact on both the dielectric constant and loss, at room temperature for Al-free and Al-doped ZnO samples.

$$\varepsilon^* = \varepsilon' - j\varepsilon'' \quad (19)$$

For all prepared samples, it's clear that the value of ε' decreased gradually when the applied frequency increased up to 10^4 Hz, then showed a frequency-independent value. This behavior may be attributed to the polarization effects and/or the number of relaxation processes [43-45]. Where the accumulations of the free charge carriers at an edge of an insulating grain boundary should exhibit large polarization effects that produce large polarization caused the dielectric constant to have a high value at the region of lower frequencies [47]. While At the region of high frequencies, the electric dipoles cannot follow the variation of the applied electric field [48, 49]. It can be observed that the dielectric constant decreases for high Al doping concentration and increases for low doping at Al 4% doping. The improved dielectric constant at room temperature makes the doped samples suitable material for charge storage applications.

Figure (12) shows the variation of ε" versus frequency for all the prepared samples. This plot depicts high values of ε" for lower frequencies, which then decreased to nearly stable values for higher frequencies. The higher ε" -values detected in the low frequencies region may be due to the crystal defects, impurities, and moisture in the prepared samples [48]. The low ε" -values at higher frequencies make the synthesized samples suitable materials for nonlinear optical applications [49]. Furthermore, materials with low values of dielectric constant and dielectric loss at higher frequencies are appropriate candidates to be utilized in devices functioning in the high-frequency range [52].

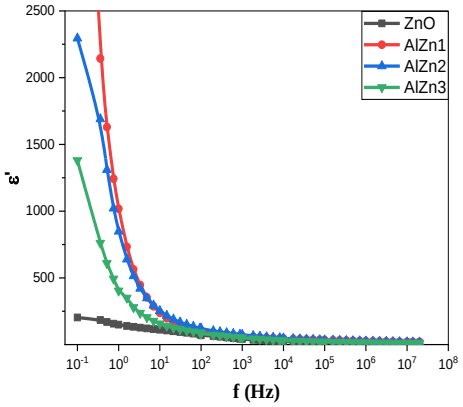

Fig. (11): Frequency dependence of optical dielectric constant for all the prepared samples, ZnO, $AlZn_1$, $AlZn_2$, and $AlZn_3$, at room temperature.

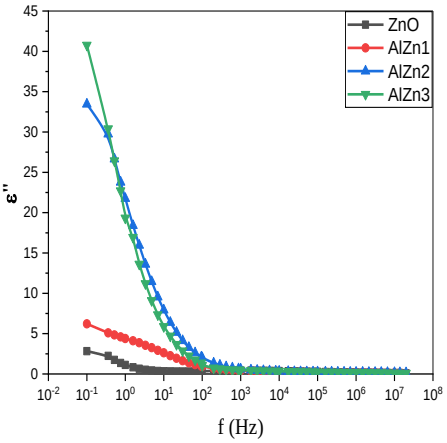

Fig. (12): Frequency dependence of optical dielectric loss for all the prepared samples, ZnO, $AlZn_1$, $AlZn_2$, and $AlZn_3$, at room temperature.

Ac Electric Conduction:

The alternating electric conduction or what is called AC conductivity is an interesting measurement, which gives an idea of the possibility of using the studied samples for electrical applications. Generally. The AC conductivity σ_{ac} of dielectric material can be calculated using the relation (20) [51], where ω is the angular frequency ($\omega = 2\pi f$) and ε_0 is the permittivity of free space ($8.854\ 10^{-12}$ F/m).

$$\sigma_{ac} = \varepsilon\varepsilon_0\, \omega\, tan\delta \quad (20)$$

Figure (13) illustrates the AC conductivity frequency dependence at room temperature for Al-free and Al-doped samples. It's clear that the AC value increased when the value of frequency increased, especially at higher frequencies. Such behavior may attribute to the migration of enhanced electrons [52]. From figure (2), it's clear that the Al impurities acted to enhance the AC conduction, especially in the region of low frequencies (less than 10^4 Hz) in which the AC-value is frequency independent, approximately. While in the region of high frequencies (up to 10^4 Hz) the AC-value increase linearly with the same rate for all samples, which means the same conduction mechanism. Such variation in AC-value between the two ranges from frequency-independent to frequency-dependent puts forward the conductivity relaxation phenomenon [53], as mentioned in the section of optical dielectric constant and loss. Generally, the behavior of AC-value with the change in the applied frequency can be understood by assume the existence of two conduction mechanisms, the first took place at the low frequencies (tunneling), while the other took place at the high frequencies (hopping) [50-58]. Also, Al-impurities acted to induce somehow of defects like zinc interstitials and oxygen vacancies throughout the ZnO nanoparticles host lattice. Such defects isolated at the grain boundaries [59-60], and facilitated the formation of a potential barrier acted to blockage of charge carriers' flow which in turn decreases conductivity [51, 59]. These results make us suggest that Al-doped ZnO nanoparticles may be considered a promising candidate for high-energy storage devices [49].

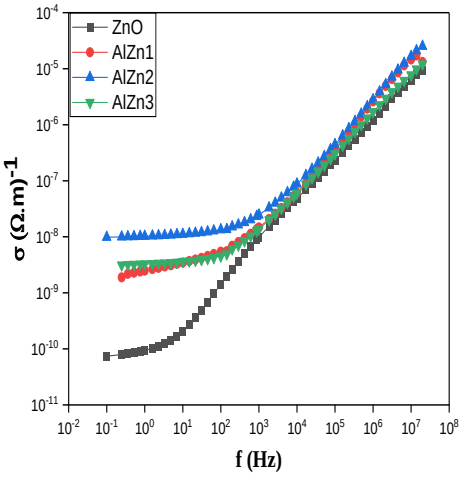

Fig. (13): Frequency dependence of ac conductivity for all prepared samples, ZnO, $AlZn_1$, $AlZn_2$, and $AlZn_3$, at room temperature

4. Conclusion:

The co-participation method is a successful method of nanopowder preparation. This method has been used to prepare Al-free and Al-doped ZnO nanopowder according to the chemical formula, $Zn_{1-x.}\, Al_x$, where $0 \leq x \leq 0.1$ %. XRD, FTIR, and UV-vis. confirmed that all samples have polycrystalline wurtzite type structure, which matching with the standard value. Al-impurities impacted the average crystalline size (D) to increase and the micro- strain to decrease. FT-IR spectra showed the vibration of Zn–O bonds as well as the incorporation of Al in ZnO nanoparticles. The Al-content caused the optical band gap to increase from 4.01 to 4.17 eV. The Al-content caused the values of the absorption coefficient and nonlinear refractive index to increase. The AC conductivity was found to depend on both the Al-content as well as the applied frequency.

Acknowledgments Not applicable.

Authors' Contributions All authors contributed to the study conception and design. Samples preparation, data collection and analysis were performed by prof. M .Y. Hassaan, Dr. Hosam. Mohamad Gomaa, Dr. F .M. Ebrahim, Dr. K. Adly. The initial draft of the manuscript was written by Dr. Nasser Moussa and all authors commented on previous versions of the manuscript. All authors read and approved the final manuscript

Funding Not applicable.

Availability of Data and Materials Not applicable.

Declarations

Competing Interests The authors have no relevant financial or non-financial interests to disclose.

List of Symbols and Abbreviations:

NPs: Nanoparticles
RT: Room Temperature
XRD: X-ray diffraction
FTIR: Fourier Transform infrared
AC: Alternating conductivity
ZnO: Al-free sample
AlZn: Al-doped sample
a, c, and c/a: Lattice parameters
δ: Dislocation
d: Inter-planer spacing
u: Positional parameter
λ: Photon wavelength
A: Optical absorbance
T%: Optical Transmittance
R%: Optical reflectance
A: Optical absorption coefficient
K: Extinction coefficient
t: sample thickness
Eg: Energy gap
c: Speed of light in space
h: Planck's constant
υ, f: photon frequency
ε1: Optical dielectric constant

ε2: Optical dielectric loss
ε': Electrical dielectric constant
ε'': Electrical dielectric loss
tanδ: Electrical loss tangent
n: Linear refractive index
n2: Nonlinear refractive index
χ(1): First optical susceptibility
χ(3): Third optical susceptibility

***References*:**

1. Coleman, V.A., Bradby, J.E., Jagadish, C., Munroe, P., Heo, Y.W., Pearton, S.J., Norton, D.P., Inoue, M. and Yano, M., Mechanical properties of ZnO epitaxial layers grown on a-and c-axis sapphire. *Applied Physics Letters*, ***86***, (20), 203105 2005.
2. Chitra, M., Uthayarani, K., Rajasekaran, N. and Girija, E.K., Preparation and characterisation of Al doped ZnO nanopowders. *Physics Procedia*, **49**, 177-182 (2013.).
3. Bouvy, C., Marine, W., Sporken, R. and Su, B.L., Nanosized ZnO confined inside a Faujasite X zeolite matrix: Characterization and optical properties. *Colloids and Surfaces A: Physicochemical and Engineering Aspects*, **300**, (1-2), 145-149 (2007).
4. Pivin, J.C., Socol, G., Mihailescu, I., Berthet, P., Singh, F., Patel, M.K. and Vincent, L., Structure and magnetic properties of ZnO films doped with Co, Ni or Mn synthesized by pulsed laser deposition under low and high oxygen partial pressures. *Thin Solid Films*, **517**, (2), 916-922 (2008).
5. Sato, K.S.K. and Katayama-Yoshida, H.K.Y.H., Material design for transparent ferromagnets with ZnO-based magnetic semiconductors. *Japanese Journal of Applied Physics*, **39**, (6B), 558 (2000).
6. Arora, A.K., Devi, S., Jaswal, V.S., Singh, J., Kinger, M. and Gupta, V.D.,"Synthesis and characterization of ZnO nanoparticles." *Oriental Journal of Chemistry* **30**, 4 1671-1679 (2014).
7. Becheri, A., Dürr, M., Lo Nostro, P. and Baglioni, P., "Synthesis and characterization of zinc oxide nanoparticles: application to textiles as UV-absorbers., *Journal of Nanoparticle Research*, **10**, (4), 679-689 (2008).
8. Serier, H., Gaudon, M. and Ménétrier, M., "Al-doped ZnO powdered materials: Al solubility limit and IR absorption properties." *Solid State Sciences*, **11**, (7), 1192-1197 (2009).
9. Zhang, B.P., Binh, N.T., Wakatsuki, K., Segawa, Y., Yamada, Y., Usami, N., Kawasaki, M. and Koinuma, H., "Formation of highly aligned ZnO tubes on sapphire (0001) substrates." *Applied Physics Letters*, **84**, (20), 4098-4100 (2004).
10. Hammarberg, E., Prodi-Schwab, A. and Feldmann, C.,"Microwave-assisted polyol synthesis of aluminium-and indium-doped ZnO nanocrystals." *Journal of colloid and interface science*, **334**, (1), 29-36 (2009).
11. Ji, L.W., Shih, W.S., Fang, T.H., Wu, C.Z., Peng, S.M. and Meen, T.H., "Preparation and characteristics of hybrid ZnO-polymer solar cells." *Journal of materials science*, **45**, (12), 3266-3269 (2010).
12. Shohany, B.G. and Zak, A.K., "Doped ZnO nanostructures with selected elements-Structural, morphology and optical properties: A review." *Ceramics International*, **46**, (5), 5507-5520 (2020).
13. Ogi, T., Hidayat, D., Iskandar, F., Purwanto, A. and Okuyama, K., "Direct synthesis of highly crystalline transparent conducting oxide nanoparticles by low pressure spray pyrolysis." *Advanced Powder Technology*, **20**, (2), 203-209 (2009).
14. Zhang, H., Yang, D., Li, S., Ma, X., Ji, Y., Xu, J. and Que, D., "Controllable growth of ZnO nanostructures by citric acid assisted hydrothermal process." *Materials Letters*, **59**, (13), 1696-1700 (2005).
15. Zhou, H.M., Yi, D.Q., Yu, Z.M., Xiao, L.R. and Li, J., "Preparation of aluminum doped zinc oxide films and the study of their microstructure, electrical and optical properties." *Thin solid films*, **515**, (17), 6909-6914 (2007).
16. Chen, K.J., Fang, T.H., Hung, F.Y., Ji, L.W., Chang, S.J., Young, S.J. and Hsiao, Y.J., "The crystallization and physical properties of Al-doped ZnO nanoparticles." *Applied surface science*, **254**, (18), 5791-5795 (2008).
17. Li, Q.H., Zhu, D., Liu, W., Liu, Y. and Ma, X.C., "Optical properties of Al-doped ZnO thin films by ellipsometry." *Applied surface science* **254**, (10), 2922-2926 (2008).
18. Ibrahim, A., Farag, M.A. and Sadeq, M.S., "Towards highly transparent tungsten zinc sodium borate glasses for radiation shielding purposes." Ceram. Int, **47**, 12079-12090 (2022).
19. Van, L.H., Hong, M.H. and Ding, J., "Structural and magnetic property of Co-doped–ZnO thin films prepared by pulsed laser deposition." *Journal of Alloys and Compounds*, **449**, (1-2), 207-209 (2008).
20. Gherab, K., Al-Douri, Y., Voon, C.H., Hashim, U., Ameri, M. and Bouhemadou, A., "Aluminum nanoparticles size effect on the optical and structural properties of ZnO nanostructures synthesized by spin-coating technique." *Results in physics*, **7**, 1190-1197 (2017).
21. Swapna, P. and Reddy, S.V., "Synthesis and Characterization of Al Doped and (Co, Al) codoped ZnO Nanoparticles via Chemical co-precipitation Method." *Asian Journal of*

Nanoscience and Materials, **2**, (1), 111-119 (2018).
22. Mallika, A.N., Reddy, A.R., Sowribabu, K. and Reddy, K.V., "Structural and optical characterization of $Zn_{0.95-x}Mg_{0.05}Al_xO$ nanoparticles." *Ceramics International*, **41**, (8), 9276-9284 (2015).
23. Kadam, P., Agashe, C. and Mahamuni, S., "Al-doped ZnO nanocrystals." *Journal of Applied Physics*, **104**, (10), 103501 (2008).
24. Park, K.C., Ma, D.Y. and Kim, K.H.,"The physical properties of Al-doped zinc oxide films prepared by RF magnetron sputtering." *Thin solid films*, **305**, (1-2), 201-209 (1997).
25. Navale, S.C., Ravi, V., Mulla, I.S., Gosavi, S.W. and Kulkarni, S.K., "Low temperature synthesis and NOx sensing properties of nanostructured Al-doped ZnO." *Sensors and Actuators B: Chemical*, **126**, (2), 382-386 (2007).
26. Reddy, A.J., Kokila, M.K., Nagabhushana, H., Chakradhar, R.P.S., Shivakumara, C., Rao, J.L. and Nagabhushana, B.M.,"Structural, optical and EPR studies on ZnO: Cu nanopowders prepared via low temperature solution combustion synthesis." *Journal of Alloys and Compounds*, **509**, (17), 5349-5355 (2011).
27. Du, S., Tian, Y., Liu, H., Liu, J. and Chen, Y.,"Calcination effects on the properties of gallium-doped zinc oxide powders." *Journal of the American Ceramic Society*, **89**, (8), 2440-2443 (2006).
28. Iqbal, A., Mahmood, A., Khan, T.M. and Ahmed, E.,"Structural and optical properties of Cr doped ZnO crystalline thin films deposited by reactive electron beam evaporation technique." *Progress in Natural Science: Materials International*, **23**, (1), 64-69 (2013).
29. Yong, Y., Su, X., Zhou, Q., Kuang, Y. and Li, X., "The $Zn_{12}O_{12}$ cluster-assembled nanowires as a highly sensitive and selective gas sensor for NO and NO2." *Scientific reports*, **7**, (1), 1-12 (2017).
30. Farouk, M., Samir, A., Ibrahim, A., Farag, M.A. and Solieman, A., "FTIR studies and optical absorption of zinc borate glasses containing WO_3", J. Appl. Phys. A, **126**, 1-8 (2020).
31. Basyooni, M.A., Shaban, M. and El Sayed, A.M.,"Enhanced gas sensing properties of spin-coated Na-doped ZnO nanostructured films." *Scientific reports*, **7**, (1), 1-12 (2017).
32. AL-Asady, Z.M., AL-Hamdani, A.H. and Hussein, M.A., "Study the optical and morphology properties of zinc oxide nanoparticles." In *AIP Conference Proceedings*, **2213**, (1), 020061 (2020).
33. Ibrahim, A. and Sadeq, M.S., "Influence of cobalt oxide on the structure, optical transitions and ligand field parameters of lithium phosphate glasses", *Ceram. Int.*, **47,** 28536-28542 (2021).
34. Gomaa, H.M., Ali, I.S., Morsy, A.S. and Sayyed, M.I.,"Linear/nonlinear optical parameters of niobium-free and niobium-doped bismuth borate glass samples." *Applied Physics A*, **126**, (5), 1-8 (2020).
35. Hassaan, M.Y., Saudi, H.A., Gomaa, H.M. and Morsy, A.S., "Optical properties of bismuth borate glasses doped with zinc and calcium oxides." *Journal of Materials and Applications*, **9**, (1), 46-54 (2020).
36. Gomaa, H.M., Hassaan, M.Y., Saudi, H.A. and Morsy, A.S.,"The influence of both Zn^{2+} and Ca^{2+} on linear and nonlinear optical parameters of some bismuth borate-based glasses." *Applied Physics A*, **126**, (5), 1-6 (2020).
37. Elkatlawy, S.M., El-Dosokey, A.H. and Gomaa, H.M., "Structural properties, linear, and non-linear optical parameters of ternary $Se_{80}Te_{(20-x)}In_x$ chalcogenide glass systems." *Bol. Soc. Esp. Cerám. Vidr.* (2020).
38. El-Mansy, M.K., Gomaa, H.M., Hendawy, N. and Morsy, A.S.,"Effect of exchange of Bi^{+3} by Nb^{+5} on the structural and optical properties of some $(BBiNb)_2O_7$ CaO oxide glasses." *Journal of Non-Crystalline Solids*, **485**, 42-46 (2018).
39. Hassanien, A.S. and Sharma, I., "Optical properties of quaternary a-$Ge_{15-x}Sb_xSe_{50}Te_{35}$ thermally evaporated thin-films: refractive index dispersion and single oscillator parameters." *Optik*, **200**, 163415 (2020).
40. Farag, M.A., Ibrahim, A., Hassaan, M.Y. and Ramadan, R.M.,"Enhancement of structural and optical properties of transparent sodium zinc phosphate glass–ceramics nano composite." *Journal of the Australian Ceramic Society*, **58**, (2), 653-661 (2022).
41. Sayyed, M.I., Ibrahim, A., Abdo, M.A. and Sadeq, M.S.,"The combination of high optical transparency and radiation shielding effectiveness of zinc sodium borate glasses by tungsten oxide additions." *Journal of Alloys and Compounds* **904**,164037 (2022).
42. Arshad, M., Ahmed, A.S., Azam, A. and Naqvi, A.H., "Exploring the dielectric behavior of Co doped ZnO nanoparticles synthesized by wet chemical route using impedance spectroscopy." *Journal of alloys and compounds*, **577**, 469-474 (2013).
43. Das, S., Das, S. and Sutradhar, S., "Effect of Gd^{3+} and Al^{3+} on optical and dielectric properties of ZnO nanoparticle prepared by two-step hydrothermal method." *Ceramics International*, **43**, (9), 6932-6941(2017).
44. Jadhav, J. and Biswas, S., "Structural and electrical properties of ZnO: Ag core-shell nanoparticles synthesized by a polymer precursor method." *Ceramics International*, **42**, (15), 16598-16610 (2016).

45. Bhakta, N. and Chakrabarti, P.K., "XRD analysis, Raman, AC conductivity and dielectric properties of Co and Mn co-doped SnO_2 nanoparticles." *Applied Physics A*, **125**, (1), 1-11 (2019).
46. Das, S., Bandyopadhyay, A., Das, S., Das, D. and Sutradhar, S., "Defect induced room-temperature ferromagnetism and enhanced dielectric property in nanocrystalline ZnO co-doped with Tb and Co.," *Journal of Alloys and Compounds*, **731**, 591-599 (2018).
47. Lakhdar, M.H., Larbi, T., Ouni, B. and Amlouk, M., "AC conductivity, dielectric relaxation and modulus behavior of Sb_2S_2O new kermesite alloy for optoelectronic applications." *Materials Science in Semiconductor Processing*, **40**, 596-601 (2015).
48. Belkhaoui, C., Mzabi, N. and Smaoui, H., "Investigations on structural, optical and dielectric properties of Mn doped ZnO nanoparticles synthesized by co-precipitation method." *Materials Research Bulletin*, **111**, 70-79 (2019).
49. Tabib, A., Sdiri, N., Elhouichet, H. and Férid, M., "Investigations on electrical conductivity and dielectric properties of Na doped ZnO synthesized from sol gel method." *Journal of alloys and compounds*, **622**, 687-694 (2015).
50. Khan, R., de Araujo, L., Irineu, C., Khan, T., Khan, A., Ullah, B. and Fashu, S., "Influence of oxygen vacancies on the structural, dielectric, and magnetic properties of (Mn, Co) co-doped ZnO nanostructures." *Journal of Materials Science: Materials in Electronics*, **29**, (12), 9785-9795 (2018).
51. Hassan, M.M., Khan, W., Azam, A. and Naqvi, A.H., "Influence of Cr incorporation on structural, dielectric and optical properties of ZnO nanoparticles." *Journal of Industrial and Engineering chemistry*, **21**, 283-291 (2015).
52. Ansari, S.A., Nisar, A., Fatma, B., Khan, W. and Naqvi, A.H., "Investigation on structural, optical and dielectric properties of Co doped ZnO nanoparticles synthesized by gel-combustion route." *Materials Science and Engineering: B*, **177**, (5), 428-435 (2012).
53. Saad, M., Stambouli, W., Sdiri, N. and Elhouichet, H., "Effect of mixed sodium and vanadium on the electric and dielectric properties of zinc phosphate glass." *Materials Research Bulletin*, **89**, 224-231 (2017).
54. Belkhaoui, C., Mzabi, N., Smaoui, H. and Daniel, P., "Enhancing the structural, optical and electrical properties of ZnO nanopowders through (Al+ Mn) doping." *Results in Physics*, **12**, 1686-1696 (2019).
55. Gürbüz, O. and Okutan, M., "Structural, electrical, and dielectric properties of Cr doped ZnO thin films: Role of Cr concentration." *Applied Surface Science*, **387**, 1211-1218 (2016).
56. Ashokkumar, M. and Muthukumaran, S., "Effect of Ni doping on electrical, photoluminescence and magnetic behavior of Cu doped ZnO nanoparticles." *Journal of Luminescence*, **162**, 97-103 (2015).
57. Ashokkumar, M. and Muthukumaran, S., "Electrical, dielectric, photoluminescence and magnetic properties of ZnO nanoparticles co-doped with Co and Cu." *Journal of Magnetism and Magnetic Materials*, **374**, 61-66 (2015).
58. Zamiri, R., Singh, B., Belsley, M.S. and Ferreira, J.M.F.,"Structural and dielectric properties of Al-doped ZnO nanostructures." *Ceramics International*, **40**, (4), 6031-6036 (2014).
59. Zamiri, R., Kaushal, A., Rebelo, A. and Ferreira, J.M.F.,"Er doped ZnO nanoplates: synthesis, optical and dielectric properties." *Ceramics International*, **40**, (1), 1635-1639 (2014).
60. Li, X., Cao, X., Xu, L., Liu, L., Wang, Y., Meng, C. and Wang, Z., "High dielectric constant in Al-doped ZnO ceramics using high-pressure treated powders." *Journal of Alloys and Compounds*, **657**, 90-94 (2016).